Journal of Alloys and Compounds 509 (2011) 6252–6256

Contents lists available at ScienceDirect

Journal of Alloys and Compounds

journal homepage: www.elsevier.com/locate/jallcom

Nitrogen-doped SiO_2–HNb_3O_8 for rhodamine B photodegradation under visible light

Xiukai Li[a,b,c,*], Huiqi Pan[a,b,c], Qingsong Hu[a,b,c], Chi Zhang[a,b,c]

[a] China-Australia Joint Research Center for Functional Molecular Materials, Jiangsu University, Zhenjiang 212013, PR China
[b] Institute of Science, Jiangsu University, Zhenjiang 212013, PR China
[c] School of Chemistry and Chemical Engineering, Jiangsu University, Zhenjiang 212013, PR China

ARTICLE INFO

Article history:
Received 1 November 2010
Received in revised form 3 March 2011
Accepted 4 March 2011
Available online 11 March 2011

Keywords:
Niobic acid
Nitrogen doping
Photocatalysis
Visible light
Dye degradation

ABSTRACT

Silica-pillared and non-pillared HNb_3O_8 samples were doped with nitrogen for rhodamine B photodegradation under visible light irradiation. The results indicate that silica pillaring could have significant impacts on the photocatalytic activity of the HNb_3O_8 sample. With expanded interlayer spacing and stronger adsorption ability to dye molecules, the SiO_2 pillared and nitrogen-doped HNb_3O_8 sample performed much better than the non-pillared counterpart. The characteristics of samples were investigated by techniques such as XRD, FT-IR, UV–visible diffuse reflectance spectroscopy, SEM, and TEM. The relationships between catalyst structure and performance were discussed.

1. Introduction

Semiconductor photocatalysis for environment remediation and solar energy conversion is a topic of great interest [1–4]. Many Ti- and Nb- based metal oxides have been revealed as good UV-type photocatalysts [5–8]. In view of better utilization of solar light, extensive efforts have been devoted to fabricating visible-light-responsive photocatalysts. The mostly adopted method to modify the UV-type photocatalysts for visible light photocatalysis is cation or anion doping [9–12]. Recently, there were also reports on single phase metal oxides that are visible light active, such as Cd_2SnO_4 [13], $BiVO_4$ [14], and Ag_2ZnGeO_4 [15].

Lamellar titanates and niobates (e.g. $K_2Ti_4O_9$, HNb_3O_8) are one type of materials constructed by stacked thin sheets built up from metal–oxygen polyhedron units. From the view point of photocatalysis, such layered configuration is favorable for the separation and transportation of photogenerated electrons and holes; moreover, the material could provide more reaction active sites at the interlayer space. Previous research demonstrated that some lamellar titanates and niobates are better photocatalysts than simple TiO_2 and Nb_2O_5, and that the acid phases (H^+-exchanged ones) could show much higher photocatalytic activities than their original salt phases [16–19]. The layered configuration of lamellar solid acids enables the materials to have unique intercalation properties [19–21]. It has been demonstrated that many organic and inorganic guest species could be intercalated into the interlayer space of lamellar solid acids, and that the obtained hybrid materials could show improved thermal stability, larger pore size, and better catalytic activity [19–23]. In the case of photocatalytic water splitting, TiO_2 or silica pillared lamellar solid acids showed notably improved activities under UV or visible light irradiation [22–24]. Recently, some transition metal oxides intercalated solid acids were reported to be visible light active [25–27]. By depositing noble metals such as Pt onto the interlayer surface, the photocatalytic activities of lamellar solid acids could be notably improved [22,28]. Nitrogen doping is one technique commonly adopted to modify wide band gap materials for visible light photocatalysis [2,11]. The intercalation property of solid acid can also have profound influence on nitrogen doping. When urea was used as a nitrogen source, it was found that the intercalation of alkaline urea species not only helped to stabilize the layered structure of solid acids but also enabled easier nitrogen doping [29,30].

There have been few reports about visible light photocatalysis over pillared solid acids. HNb_3O_8 is a simple lamellar niobic acid with protonic acidity stronger than that of titanic acid. Nitrogen-doped HNb_3O_8 exhibited superior photocatalytic activity than nitrogen-doped Nb_2O_5 and KNb_3O_8 under visible light [29,30]. Thus it is very intriguing to further modify the nitrogen-doped HNb_3O_8 for better activity. In the present study, HNb_3O_8 was purposely

* Corresponding author at: Institute of Science, Jiangsu University, No. 301 Xuefu Rd., Zhenjiang 212013, PR China. Tel.: +86 511 88797815; fax: +86 511 88797815.
E-mail address: li.xiukai@gmail.com (X. Li).

0925-8388/$ – see front matter © 2011 Elsevier B.V. All rights reserved.
doi:10.1016/j.jallcom.2011.03.033

pillared with silica and then doped with nitrogen for visible light photocatalysis. The physico-chemical properties of samples and the effect of silica pillaring on the photocatalytic activity were investigated in detail.

2. Experimental

The HNb_3O_8 solid acid was prepared by reacting KNb_3O_8 with nitric acid [31,32]. KNb_3O_8 was first prepared by heating a mixture of Nb_2O_5 and K_2CO_3 in a molar ratio of 3:1 at 900 °C for 10 h. The KNb_3O_8 sample was then stirred in nitric acid (5 mol L^{-1}, 60 ml per gram of KNb_3O_8) at room temperature for 2 days for the generation of HNb_3O_8. The HNb_3O_8 sample recovered from the acid solution was washed thoroughly with distilled water and then dried at 70 °C for 12 h. The SiO_2 pillared HNb_3O_8 sample was prepared by the two-step ion-exchange method [31]; *n*-dodecylamine and tetraethyl orthosilicate (TEOS) were used as, respectively, the pre-expanding reagent and silicon source. The *n*-dodecylamine and TEOS intercalated samples were designated as C_{12}-HNb_3O_8 and TEOS-HNb_3O_8, respectively. The TEOS-HNb_3O_8 sample was calcined at 500 °C for 4 h in air for the formation of SiO_2 pillared HNb_3O_8 (designated as SiO_2–HNb_3O_8). The nitrogen doping of HNb_3O_8 and SiO_2–HNb_3O_8 was performed according to the procedure described previously [29,30], and urea was used as a nitrogen source. Taking the doping of HNb_3O_8 for an example, HNb_3O_8 (1.0 g) was finely ground with urea (2.0 g), and then this combination was heated in a covered crucible at 400 °C for 2 h. The yellow-colored product was crushed, washed well with diluted nitric acid and distilled water, and then dried at 70 °C overnight. The nitrogen-doped samples were designated as HNb_3O_8–N and SiO_2–HNb_3O_8–N, respectively.

The phase compositions of samples were identified by X-Ray Powder Diffraction (Cu K_α radiation, Bruker AXS-D8) in the 2θ range of 3–90°. The UV–visible diffuse reflectance spectra were recorded at room temperature on a Shimadzu UV-2450 UV–vis spectrometer with barium sulfate as the reference sample. Specific surface areas of samples were deduced by the BET method (N_2 adsorption) with a NOVA-2000E instrument. FT-IR spectra of the samples were collected on a Nicolet Nexus 470 FT-IR spectrophotometer at room temperature by KBr method. Morphologies of samples were characterized using a scanning electron microscope (JSM-7001F, JEOL) and a high resolution transmission electron microscope (HR JEM-2100, JEOL).

In the activity test, 0.2 g catalyst was suspended in 100 ml rhodamine B (RhB) aqueous solution (10.0 mg L^{-1}, PH value: 7) in a pyrex reactor. The suspension was stirred in the dark for about 40 min before light was turned on. A 350 W Xe-lamp (Nanshen Company, Shanghai) equipped with UV cutoff filter ($\lambda > 400$ nm) and a water filter was used as light source. The average intensity of the incident light was ca. 50.0 mW cm^{-2}. At given irradiation time intervals, 3 ml of the reaction mixture was sampled, and separated by filtration. The concentration of RhB was determined by monitoring the changes in the absorbance maximized at 554 nm.

3. Results and discussion

HNb_3O_8 is isostructural with KNb_3O_8 and is crystallized in an orthorhombic symmetry [29,33]. It has layered structure constructed of 2D $Nb_3O_8^-$ anion slices built by corner- and edge-sharing NbO_6 octahedra, the H^+ cations are located between the slices. Fig. 1 shows the XRD patterns of HNb_3O_8 and the intercalated derivatives. The 020 diffraction peak at $2\theta = 7.8°$ for HNb_3O_8 is characteristic of the layered structure, and the *d* value (ca. 11.3 Å) corresponds to the interlayer distance. Intercalation of guest components at the interlayer space notably changed the interlayer distance of HNb_3O_8. From Fig. 1b one can see that the interlayer distance d_{020} was remarkably expanded to 30.2 Å after *n*-dodecylamine intercalation. The interlayer distance d_{020} further increased to 36.8 Å after the sample was reacted with TEOS (Fig. 1c). Upon heating at 500 °C for 4 h in air, the intercalated TEOS transformed to SiO_2. As seen from Fig. 1d, the 0 2 0 diffraction peak was clearly observed for the SiO_2–HNb_3O_8 sample, signifying that the silica pillars were formed and the layered structure was well retained for the host material. In contrast, pure HNb_3O_8 is thermally unstable and usually decomposes to *R*′-Nb_2O_5 at temperatures above 200 °C [29,30]. The d_{020} value (30.2 Å) of SiO_2–HNb_3O_8 is much larger than that (11.3 Å) of non-pillared HNb_3O_8; the value is also lager than that (25.3 Å) of a silica pillared HNb_3O_8 sample prepared with *n*-decylamine as pre-expanding reagent [31], probably because of the longer chain length of *n*-dodecylamine used in this study. Taking into account the thickness of the $Nb_3O_8^-$ anion slice is 7.5 Å [31], the interlayer spacing of SiO_2–HNb_3O_8 was calculated to be 22.7 Å (30.2 Å subtract 7.5 Å), contrast to only 3.8 Å (11.3 Å subtract 7.5 Å) of HNb_3O_8. Owing to the notably expanded interlayer distance, the surface area value of SiO_2–HNb_3O_8 was as large as 220.1 $m^2\ g^{-1}$, contrasted to only 7.2 $m^2\ g^{-1}$ of the non-pillared sample.

Fig. 2 shows the FT-IR spectra of HNb_3O_8 and its intercalated derivatives. The IR absorption in the range of 400–1000 cm^{-1} is assigned to the vibration of the $Nb_3O_8^-$ host slice [31]. Absorptions in the range of 2853–2957 cm^{-1} and 1394–1507 cm^{-1} observed for C_{12}–HNb_3O_8 (Fig. 2b) and TEOS–HNb_3O_8 (Fig. 2c) are ascribed to, respectively, the C–H symmetric/asymmetric stretching and C–H bending of the intercalated organic guests [31,34]. Additional absorptions at 1077 cm^{-1} attributable to the vibration of Si–O–Si linkages [31,34] were also observed for TEOS-HNb_3O_8 (Fig. 2c) and SiO_2–HNb_3O_8 (Fig. 2d), indicating that siliceous species (TEOS or SiO_2) have successfully intercalated into the host material. The absorptions of C-H stretching and bending models were not observed for SiO_2–HNb_3O_8, signifying that the intercalated organic species were completed decomposed after the sample was heated at 500 °C for 4 h in air. The spectrum of nitrogen-doped SiO_2–HNb_3O_8 is also shown (Fig. 2e). Compared with the spectrum of undoped SiO_2–HNb_3O_8 (Fig. 2d), the IR absorption assignable to the $Nb_3O_8^-$ host slice (400–1000 cm^{-1}) is almost unchanged for

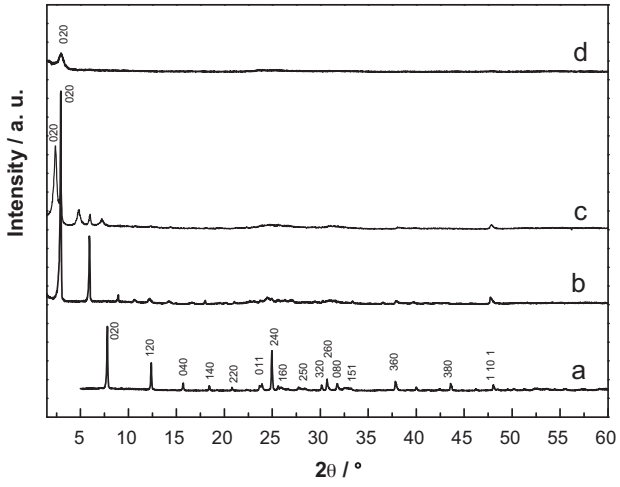

Fig. 1. XRD patterns of (a) HNb_3O_8; (b) C_{12}–HNb_3O_8; (c) TEOS–HNb_3O_8; (d) SiO_2–HNb_3O_8.

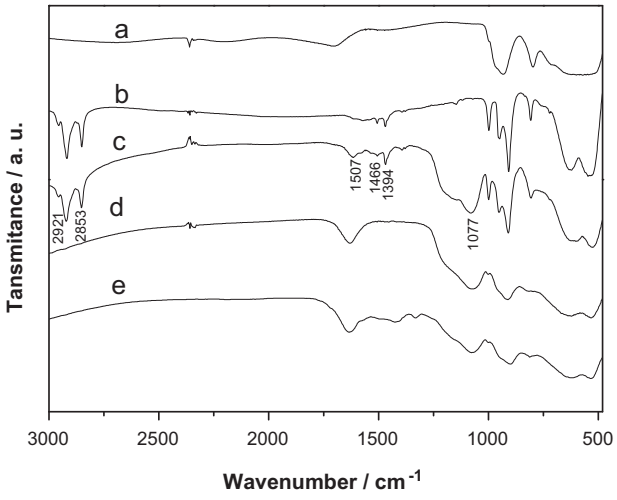

Fig. 2. FT-IR spectra of (a) HNb_3O_8; (b) C_{12}–HNb_3O_8; (c) TEOS–HNb_3O_8; (d) SiO_2–HNb_3O_8; (e) SiO_2–HNb_3O_8–N.

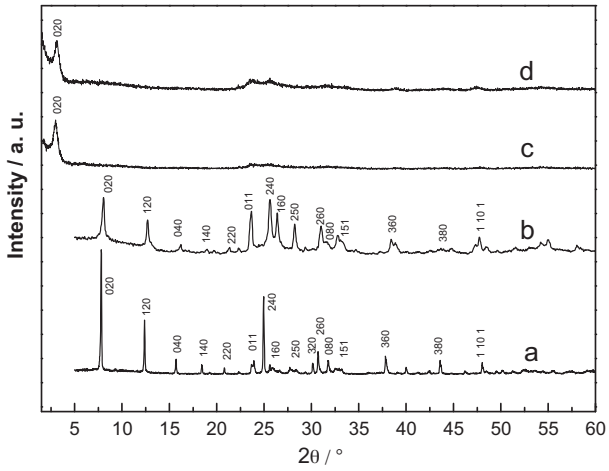

Fig. 3. XRD patterns of (a) HNb_3O_8; (b) HNb_3O_8–N; (c) SiO_2–HNb_3O_8; (d) SiO_2–HNb_3O_8–N.

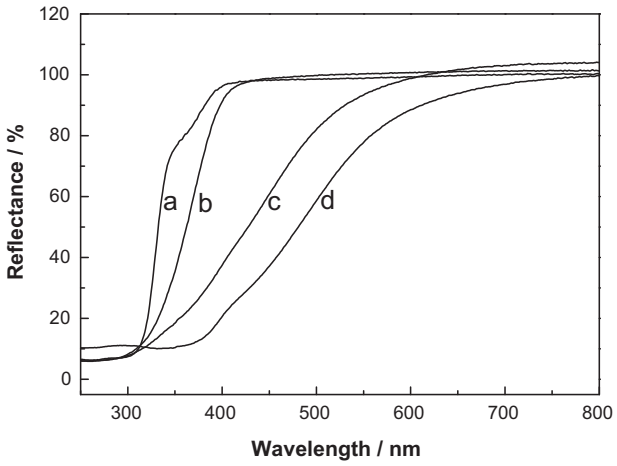

Fig. 5. Diffuse reflectance spectra of (a) HNb_3O_8; (b) SiO_2–HNb_3O_8; (c) SiO_2–HNb_3O_8–N; (d) HNb_3O_8–N.

SiO_2–HNb_3O_8–N, signifying that the structure of the HNb_3O_8 host was basically retained after nitrogen doping.

Fig. 3 shows the XRD patterns of the nitrogen-doped and undoped HNb_3O_8 and SiO_2–HNb_3O_8 samples. All the samples were doped with nitrogen by the solid state-reaction method with urea as a nitrogen source. As seen from Fig. 3b, the layered structure was well retained for the HNb_3O_8 sample after nitrogen doping. It was proposed that the intercalation of alkaline urea helped to stabilize the layered structure of HNb_3O_8 during the heating process [29,30]. From Fig. 3c and d one can see that the phase composition and peak intensity was almost unchanged for SiO_2–HNb_3O_8–N, signifying that the SiO_2–HNb_3O_8 sample is stable in nitrogen doping.

The morphologies of samples were investigated by the scanning electron microscopy (SEM) and transmission electron microscopy (TEM), and the images of samples were shown in Fig. 4. Shown in Fig. 4A is the SEM image of HNb_3O_8 containing a number of micron-sized particles. After the sample was pillared with silica, the morphology of SiO_2–HNb_3O_8 changed from irregular particles to thin flakes with thickness of about 100 nm (Fig. 4B); this change might be due to the exfoliation and aggregation of the $Nb_3O_8^-$ nano-sheets during the sample synthesis process. Figs. 4C and D shows the TEM images of undoped and nitrogen doped SiO_2–HNb_3O_8 samples, respectively. The layered texture could be clearly observed for both samples, and this further support that the SiO_2–HNb_3O_8 sample is stable in the process of nitrogen doping.

Nitrogen doping is one of the most commonly used methods to modify UV-type photocatalysts for visible light photocatalysis. Gaseous ammonia, melamine, and urea could be used as nitrogen source [2,29,30,35–40]. Compared with gaseous ammonia, urea is easier to handle and control, and therefore was used as nitrogen source in the present study. Fig. 5 shows the reflectance spectra of the nitrogen-doped and undoped samples. The undoped HNb_3O_8 and SiO_2–HNb_3O_8 samples are white colored and absorb only the UV light. The band gaps were estimated from the onsets of the sharp absorption edges and the values are 3.5 eV and 3.1 eV for HNb_3O_8 and SiO_2–HNb_3O_8 (Table 1), respectively. The lowering of

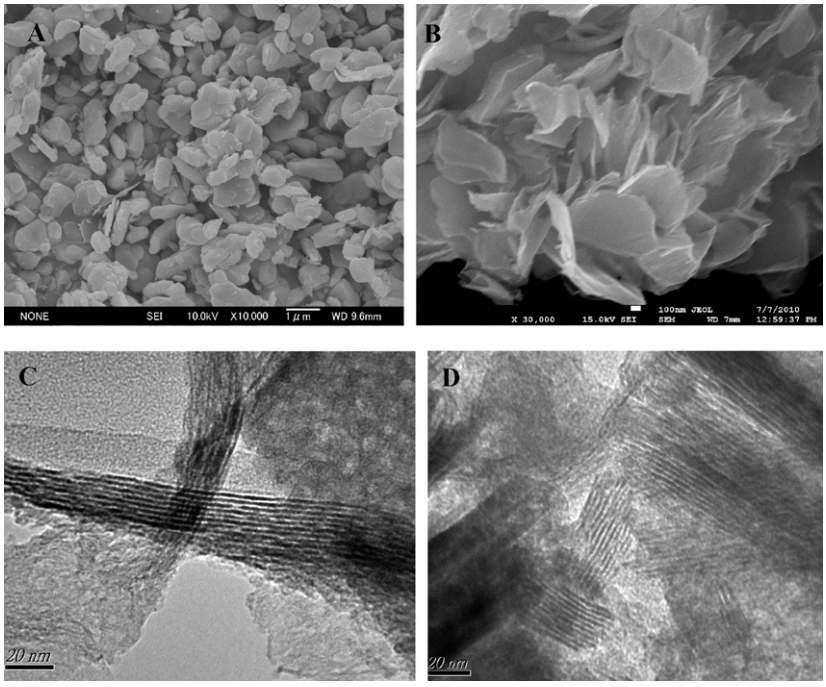

Fig. 4. SEM images of (A) HNb_3O_8 and (B) SiO_2–HNb_3O_8; TEM images of (C) SiO_2–HNb_3O_8 and (D) SiO_2–HNb_3O_8–N.

Table 1
Physical characteristics of samples.

Samples	d_{020} (Å)	Interlayer spacing (Å)	Band gap (eV)[a]
HNb_3O_8	11.3	3.8	3.5
HNb_3O_8–N	11.0	3.5	2.1
SiO_2–HNb_3O_8	30.2	22.7	3.1
SiO_2–HNb_3O_8–N	28.5	21.0	2.3

[a] The band gap values were calculated according to the following equation: Eg: $hC/\lambda_{os} = 1240\,eV/\lambda_{os}$ (h: Plank constant; C: the speed of light in vacuum). λ_{os} means the onset absorption; it was taking from the DRS curve shown in Fig. 5.

the band gap from HNb_3O_8 to SiO_2–HNb_3O_8 might be due to the partial dehydration of the host part of SiO_2–HNb_3O_8 in the process of sample preparation. The HNb_3O_8–N and SiO_2–HNb_3O_8–N samples are yellow colored and show obvious absorption in the visible region. Compared with the undoped ones, the absorption edges of HNb_3O_8–N and SiO_2–HNb_3O_8–N shift notably to the longer wavelength end, and the band gaps were estimated to be 2.1 eV and 2.3 eV, respectively. The significant reduction in the band gap caused by nitrogen doping is probably due to the particular properties of lamellar solid acid and the using of urea as a nitrogen precursor. It was revealed that the intercalation of urea to lamellar solid acids could facilitate nitrogen doping in larger amount into the thin anion slices of the solid acid [29,30]. Nitrogen doping could shift the top of valence band to a more negative position and leads to a narrowed band gap [2]. The HNb_3O_8–N sample absorbs more visible light than SiO_2–HNb_3O_8–N, signifying that more nitrogen atoms were doped into the former sample. Since the SiO_2–HNb_3O_8 sample has been heated at 500 °C for 4 h during the preparation process, it should be partially dehydrated and thus possesses fewer protons at the interlayer space than the non-pillared one. As a consequence the interaction between SiO_2–HNb_3O_8 and urea should be lower than that in the HNb_3O_8 case, and therefore less nitrogen atoms were doped into the $Nb_3O_8^-$ slices of SiO_2–HNb_3O_8. Because the atomic diameters and the number of valence electrons of N and O are different, larger amount of N doping would result in defect sites and non-stoichiometry in the material. Generally, there is an optimum amount of doped N to achieve the best activity [35,36]. It was reported that codoping with cations and anions could depress the formation of defect sites and enhance the photocatalytic activity [41].

In the present study, the HNb_3O_8–N and SiO_2–HNb_3O_8–N samples were evaluated for rhodamine B (RhB) photodegradation in neutral aqueous solution under visible light ($\lambda > 400$ nm) irradiation. As shown in Fig. 6, the photolysis of RhB (without any catalyst) under visible light irradiation was very slow, and less than 5% of RhB was converted after 120 min of irradiation. The SiO_2–HNb_3O_8–N sample showed stronger adsorption ability to RhB than HNb_3O_8–N, possibly because of its much greater surface area. Approximately 64.2% RhB was adsorbed on SiO_2–HNb_3O_8–N when the adsorption–desorption equilibrium was established; in contrast, only 16.4% RhB was adsorbed on HNb_3O_8–N. The concentration of RhB decreased continuously with visible light irradiation. Over the SiO_2–HNb_3O_8–N sample ca. 98% of RhB was converted after 80 min of irradiation, while over the HNb_3O_8–N sample the same extent of RhB conversion took more than 140 min. The pictures of the RhB solution before and after photocatalytic reaction over the SiO_2–HNb_3O_8–N sample are shown in Fig. 7. From Fig. 7 one can see that, after 80 min of visible light irradiation, not only RhB in the solution phase but also the RhB molecules adsorbed on the surface of SiO_2–HNb_3O_8–N were degraded. While over the HNb_3O_8–N sample, after the same irradiation time the reaction suspension was still red (the picture is not shown). It is evident that over the SiO_2–HNb_3O_8–N sample RhB was indeed degraded instead of being simple adsorbed on sample surface. A nitrogen-doped anatase phase TiO_2 was prepared by the same method and was evaluated for comparison. As shown in Fig. 6, under identical reaction conditions, the SiO_2–HNb_3O_8–N sample also performed much better than nitrogen-doped TiO_2. The current study demonstrated that by pillaring with silica the activity of HNb_3O_8–N could be notably improved. Firstly, dye molecules can be oxidized or be reduced directly on the surface of photocatalysts, thus the stronger adsorption ability of the SiO_2–HNb_3O_8–N sample should contribute to a higher activity. As dye photodegradation in liquid phase usually follow the pseudo-first-order [3], the stronger adsorption ability of SiO_2–HNb_3O_8–N enhanced the concentration of RhB on sample surface, and this certainly contributed to a higher rate of RhB conversion. Secondly, it was revealed that the reaction active sites of lamellar solid acids lie at the interlayer surface of the materials [22,28]. With notably expanded interlayer distance, the reaction active sites at the interlayer space of SiO_2–HNb_3O_8–N should be more accessible to the reaction substrates. Water molecules can also be more easily intercalated into the SiO_2–HNb_3O_8–N sample. The intercalated water molecules could trap the photoexcited holes at the interlayer surface to form the active hydroxyl radicals ($OH^\bullet$), this facilitates the separation of electron–hole pairs

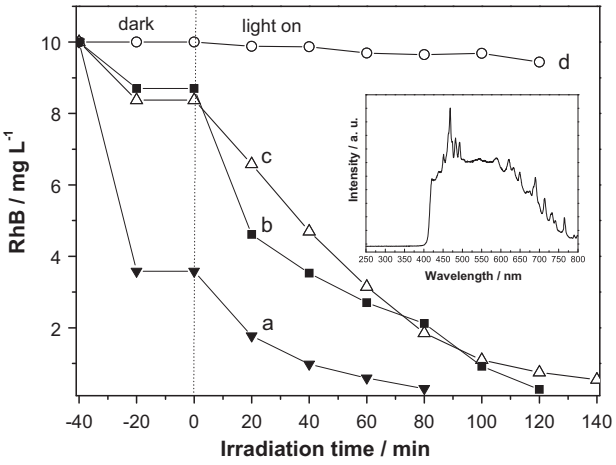

Fig. 6. Photocatalytic degradation of RhB over: (a) SiO_2–HNb_3O_8–N; (b) TiO_2–N; (c) HNb_3O_8–N. The photolysis of RhB (line d) was also shown for comparison. The inset shows the wavelength distribution of the incident light applied in activity test. The average intensity of the irradiation light was ca. 50.0 mW cm^{-2}.

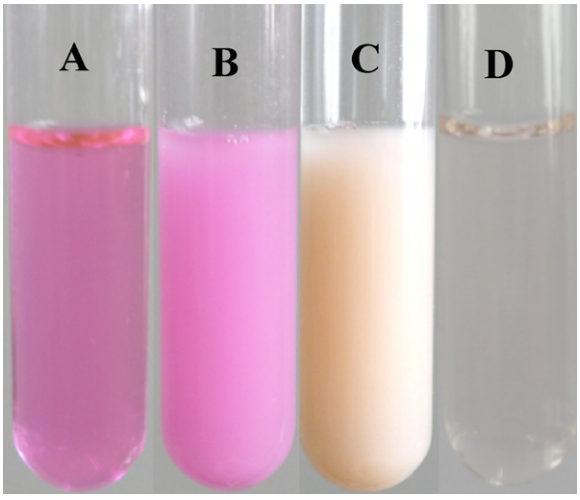

Fig. 7. Pictures of RhB solution. (A) The original RhB solution (10 mg L^{-1}); (B) the reaction mixture (with the SiO_2–HNb_3O_8–N photocatalyst) before light irradiation; (C) the reaction mixture after 80 min of visible light ($\lambda > 400$ nm) irradiation; (D) the filtrate of (C).

and accounts in certain extent for the higher photocatalytic activity. Lastly, since SiO_2–HNb_3O_8–N was doped with smaller amount of nitrogen atoms, the sample should possess less lattice oxygen defects. Because of the same reason, the valence band top of SiO_2–HNb_3O_8–N did not shift toward the negative potential as much as that of HNb_3O_8–N (Fig. 5); as a consequence the photogenerated holes at the valence band of SiO_2–HNb_3O_8–N should have stronger oxidation ability than that in HNb_3O_8–N, and this might also contribute partly to the higher activity of SiO_2–HNb_3O_8–N. In summary, the SiO_2–HNb_3O_8 sample possesses particular properties like larger surface area, expanded interlayer space, and better nitrogen doping character; these aspects contributed to the overall activity of the SiO_2–HNb_3O_8–N photocatalyst.

4. Conclusions

Silica-pillared and non-pillared HNb_3O_8 samples were doped with nitrogen for RhB photodegradation under visible light irradiation. As a result of silica pillaring, the interlayer spacing of SiO_2–HNb_3O_8 was expanded from 3.8 to 22.7 Å, and the surface area value of the sample increased from 7.2 to 220.1 $m^2\,g^{-1}$. The SiO_2–HNb_3O_8–N and HNb_3O_8–N samples showed good absorption in visible region after nitrogen doping, and their band gaps were 2.3 eV and 2.1 eV, respectively. SiO_2–HNb_3O_8–N showed stronger adsorption ability to RhB than HNb_3O_8–N, over the former sample 64.2% RhB was adsorbed while over the latter sample 16.4% RhB was adsorbed. With expanded interlayer spacing, better adsorption ability and optical property, the SiO_2–HNb_3O_8–N sample performed much better than HNb_3O_8–N. Approximately, 98% RhB was degraded over SiO_2–HNb_3O_8–N after 80 min of visible light irradiation, while over HNb_3O_8–N the same extent of RhB degradation took more than 140 min. The present study enables a deeper understanding about the chemistry and photocatalysis over silica-pillared lamellar solid acid.

Acknowledgements

This research was supported by the National Natural Science Foundation of China (No. 21003064) and the Research Foundation of Jiangsu University (No. 1283000372/3).

References

[1] K. Maeda, K. Teramura, D. Lu, T. Takata, N. Saito, Y. Inoue, K. Domen, Nature 440 (2006) 295.
[2] R. Asahi, T. Morikawa, T. Ohwaki, K. Aoki, Y. Taga, Science 293 (2001) 269–271.
[3] X. Li, J. Ye, J. Phys. Chem. C 111 (2007) 13109–13116.
[4] M. Zhang, H. Yang, T. Xan, Z.Q. Wei, J.L. Jiang, Y.C. Feng, X.Q. Liu, J. Alloys Compd. 509 (2011) 809–812.
[5] Z. Yu, S.S.C. Chuang, Appl. Catal. B 83 (2008) 277–285.
[6] N. Quici, M.L. Vera, H. Choi, G.L. Puma, D.D. Dionysiou, M.I. Litter, H. Destaillats, Appl. Catal. B 95 (2010) 312–319.
[7] T. Puangpetch, T. Sreethawong, S. Yoshikawa, S. Chavadej, J. Mol. Catal. A 312 (2009) 97–106.
[8] M.Y. Guo, M.K. Fung, F. Fang, X.Y. Chen, A.M.C. Ng, A.B. Djurisic, W.K. Chan, J. Alloys Compd. 509 (2011) 1328–1332.
[9] D. Wang, J. Ye, T. Kako, T. Kimura, J. Phys. Chem. B 110 (2006) 15824–15830.
[10] J.R. Konta, T. Ishii, H. Kato, A. Kudo, J. Phys. Chem. B 108 (2004) 8992–8995.
[11] S.M. Ji, P.H. Borse, H.G. Kim, D.W. Hwang, J.S. Jang, S.W. Bae, J.S. Lee, Phys. Chem. Chem. Phys. 7 (2005) 1315–1321.
[12] D. Wu, M. Long, W. Cai, C. Chen, Y. Wu, J. Alloys Compd. 502 (2010) 289–294.
[13] X. Huang, J. Lv, Z. Li, Z. Zou, J. Alloys Compd. 507 (2010) 341–344.
[14] C. Chung, C. Lu, J. Alloys Compd. 502 (2010) L1–L5.
[15] X. Li, S. Ouyang, N. Kikugawa, J. Ye, Appl. Catal. A 334 (2008) 51–58.
[16] J. Yosbimura, Y. Ebina, J. Kondo, K. Domen, J. Phys. Chem. 97 (1993) 1970–1973.
[17] L. Zhang, W. Zhang, L. Lu, X. Yang, X. Wang, J. Mater. Sci. 41 (2006) 3917–3921.
[18] K. Domen, J. Yoshimura, T. Sekine, A. Tanakaa, T. Onishi, Catal. Lett. 4 (1990) 339–344.
[19] K. Domen, Y. Ebina, T. Sekine, A. Tanakaa, J. Kondo, C. Hirose, Catal. Today 16 (1993), 479–466.
[20] X. Wang, W. Hou, H. Wang, Q. Yan, Catal. Commun. 3 (2002) 275–280.
[21] X. Wang, W. Hou, Q. Yan, Chem. Lett 3 (2001) 188–189.
[22] S. Yin, D. Maeda, M. Ishitsuka, J. Wu, T. Sato, Solid State Ionics 151 (2002) 377–383.
[23] X. Li, B. Yue, J. Ye, Appl. Catal. A 390 (2010) 195–200.
[24] Y. Ebina, A. Tanaka, J.N. Kondo, K. Domen, Chem. Mater. 8 (1996) 2534–2538.
[25] T.W. Kim, S. Hwang, S.H. Jhung, J. Chang, H. Park, W. Choi, J. Choy, Adv. Mater. 20 (2008) 539–542.
[26] T.W. Kim, S.G. Hur, S. Hwang, H. Park, W. Choi, J. Choy, Adv. Funct. Mater. 17 (2007) 307–314.
[27] J. Wu, Y. Cheng, J. Lin, Y. Huang, M. Huang, S. Hao, J. Phys. Chem. C 111 (2007) 3624–3628.
[28] T. Takata, A. Tanaka, M. Hara, J.N. Kondo, K. Domen, Catal. Today 44 (1998) 17–26.
[29] X. Li, N. Kikugawa, J. Ye, Adv. Mater. 20 (2008) 3816–3819.
[30] X. Li, N. Kikugawa, J. Ye, Chem. Eur. J. 15 (2009) 3538–3545.
[31] X. Guo, W. Hou, W. Ding, Y. Fan, Q. Yan, Y. Chen, Micropor. Mesopor. Mater. 80 (2005) 269–274.
[32] X. Jing, Y. Li, Q. Yang, Q. Yin, Mater. Sci. Eng. B 110 (2004) 18–22.
[33] R. Nedjar, M.M. Borel, B. Raveau, Mater. Res. Bull. 20 (1985) 1291–1296.
[34] W. Hou, L. Xu, Q. Yan, J. Chen, Chin. J. Inorg. Chem. 18 (2002) 744–745.
[35] T. Murase, H. Irie, K. Hashimoto, Phys. Chem. B 108 (2004) 15803–15807.
[36] H. Shi, X. Li, H. Iwai, Z. Zou, J. Ye, J. Phys. Chem. Solid 70 (2009) 931–935.
[37] M. Sathish, B. Viswanathan, R.P. Viswanath, Appl. Catal. B 74 (2007) 307–312.
[38] K. Kobayakawa, Y. Murakami, Y. Sato, Photochem. Photobio. A 170 (2005) 177–179.
[39] J. Wang, S. Yin, M. Komatsu, Q. Zhang, F. Saito, T. Sato, Appl. Catal. B 52 (2004) 11–21.
[40] K.R. Reyes-Gil, Y. Sun, E. Reyes-Garcia, D. Raftery, J. Phys. Chem. C 113 (2009) 12558–12570.
[41] M. Miyauchi, M. Takashio, H. Tobimatsu, Langmuir 20 (2004) 232–236.